Hindawi
Science and Technology of Nuclear Installations
Volume 2018, Article ID 5808352, 12 pages
https://doi.org/10.1155/2018/5808352

Research Article

Design of the Online Gross γ Monitoring Instrument at the Exit of the Helium Purification System in HTR-PM

Mengqi Lou,[1,2] Liguo Zhang,[1] Feng Xie,[1] Jianzhu Cao,[1] Jiejuan Tong,[1] Weirong Liu,[3] and Yong Wang[3]

[1]*Institute of Nuclear and New Energy Technology, Collaborative Innovation Center of Advanced Nuclear Energy Technology, Key Laboratory of Advanced Reactor Engineering and Safety of Ministry of Education, Tsinghua University, Beijing 100084, China*
[2]*Division of Nuclear Power Safety, Royal Institute of Technology (KTH), SE-106 91 Stockholm, Sweden*
[3]*China Nuclear Power Engineering Co., Ltd., Beijing 100840, China*

Correspondence should be addressed to Feng Xie; fxie@tsinghua.edu.cn

Received 16 June 2018; Accepted 2 October 2018; Published 1 November 2018

Academic Editor: Arkady Serikov

After the successful construction and operation experience of the 10 MW high-temperature gas-cooled reactor (HTR-10), a high-temperature gas-cooled pebble-bed modular (HTR-PM) demonstration plant is under construction in Shidao Bay, Rongcheng City, Shandong province, China. An online gross γ monitoring instrument has been designed and placed at the exit of the helium purification system (HPS) of HTR-PM and is used to detect the activity concentration in the primary circuit after purification. The source terms in the primary loop of HTR-PM and the helium purification process were described. The detailed configuration of the gross γ monitoring instrument was presented in detail. The Monte Carlo method was used to simulate the detection efficiency of the monitoring system. Since the actual source terms in the primary loop of HTR-PM may be different than the current design values, a sensitivity analysis of the detection efficiency was implemented based on different relative proportions of the nuclides. The accuracy and resolution of the NaI(Tl) detector were discussed as well.

1. Introduction

Generation IV nuclear energy systems were introduced 16 years ago. The very-high-temperature reactor (VHTR), as an advanced type of the high-temperature gas-cooled reactors (HTGRs), is one of the six Generation IV nuclear energy systems. The VHTR offers promising perspectives for hydrogen production due to the high coolant outlet temperatures, which can be above 1000°C [1]. 53 reactors were under construction worldwide on July 1st, 2017, and 20 of them were in China [2].

The research and design program of HTGRs started in the 1940s. The UK, Germany, the USA, and Japan have built test or prototype reactors for over seven decades. In China, the Institute of Nuclear and New Energy Technology (INET), at Tsinghua University, has conducted the research and development of HTGRs. The basic theoretical and experimental research on HTGRs has started in the 1970s [3–5]. The construction of the first Chinese high-temperature gas-cooled pebble-bed test reactor, the 10 MW high-temperature gas-cooled reactor (HTR-10), started in 1995. The reactor reached its criticality in 2000, and researchers have conducted four experiments to verify its inherent safety characteristics by 2007 [3–5]. Based on the successful operation of HTR-10, the construction of the high-temperature gas-cooled pebble-bed modular (HTR-PM) demonstration plant started at the end of 2012 to verify the technologies and to confirm the feasibility and reliability of modularized reactors, which are crucial steps to demonstrate whether HTRs can economically compete against light water reactors (LWRs). Both HTR-10 and HTR-PM use helium as the coolant and graphite as moderator. The spherical fuel elements are tristructural-isotropic (TRISO) coated particles embedded in the graphite matrix, while the mean free uranium fraction of five consecutive batches is lower than 10^{-5} [6]. The HTR-PM possesses two modules, whose total thermal power and electrical outputs are 500 and 200 MW, respectively [3].

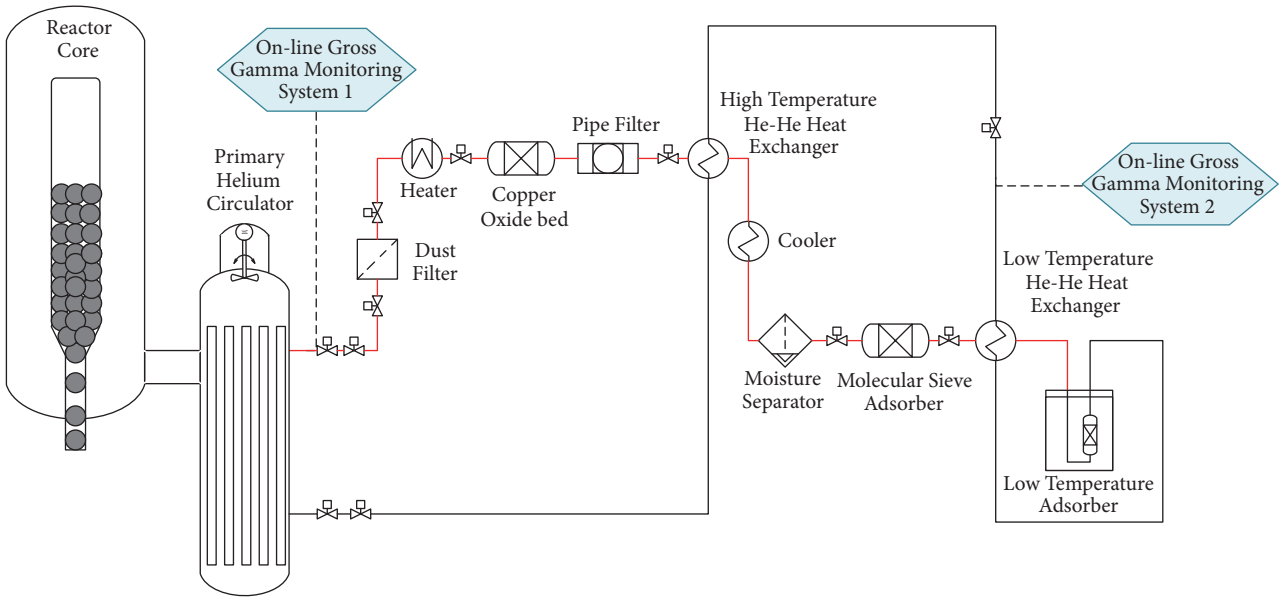

Figure 1: Configuration of the HPS and position of the online γ monitoring system.

Radiation safety of nuclear power plants has been receiving increasing attention in recent years. Radiation monitoring systems can help monitor the radiation levels for selected processes, areas, effluents, environment, and personnel, helping operators to evaluate plant conditions and take appropriate actions. With the development of detecting technology, LWRs use the online monitoring systems to detect the neutron flux, power distribution, fuel failure, and other parameters in the reactor core more often [7]. CANDU reactors adopt serial online monitoring systems to detect fuel failures [8]. Advanced Gas Reactors (AGRs) tend to set online monitoring systems to detect fuel failure during fuel testing [9]. Typically, such monitoring system may consist of five parts: the process, area, effluent, personnel, and environmental radiation monitoring systems. In HTR-PM, the individual process and effluent radiation monitoring systems were integrated into a single process and effluent radiation monitoring system [10]. The process and effluent radiation monitoring system in HTR-PM was designed based on the source term research of HTR-10, including the experimental measurement of the activity concentration of H-3 and C-14 in the primary loop [11], radioactive dust concentration in the primary loop [12–14], and types and distributions of typical nuclides in the irradiated graphite spheres from the core [15–17]. The source terms in the primary loop of HTR-PM, which contains fission and activation products, radioactive dust, H-3, and C-14, have been designed to be monitored using the online monitoring instrument and/or the sampling measurement [10, 18, 19].

Online monitoring systems can be used as important complementary systems to the existing offline sampling monitoring systems and can reflect the real-time situation of the fuel elements in the reactor core in time [7]. For HTR-PM, we adopted online monitoring techniques to continuously record the activity concentration of the fission products in the primary loop. Online gross γ monitoring instruments have been designed for the entrance and exit of the helium purification system (HPS) in the primary loop of HTR-PM. In this study, we introduced the design idea of the online monitoring instrument at the exit of the HPS. Moreover, we described the source term in the primary loop and the function of the HPS of the HTR-PM. The configuration of the monitoring instrument was also illustrated in detail. The Monte Carlo method was used to simulate the detection efficiency of the online monitoring instrument and attest to the feasibility of this design scheme. Since the source term in the primary loop of HTR-PM may vary from current calculations, a sensitivity analysis was implemented to determine the key factors that can affect detection efficiency. The improvement of the current design scheme was also discussed.

2. Configuration of the Online Gross γ Monitoring Instrument

The HPS of HTR-PM is similar to that of HTR-10 and consists of a moisture separator, dust filter, copper oxide bed, molecular sieve absorber, low-temperature absorber, etc. The HPS is a bypass of the primary circuit and its purpose is to remove both gaseous and solid impurities from the primary coolant helium. Gaseous impurities include hydrogen, carbon monoxide, carbon dioxide, water vapor, methane, and gaseous fission products including krypton, xenon, argon, and iodine, as well as solid impurities containing radioactive graphite dust and solid fission products [20]. The HPS of HTR-PM, which has a 40 $kg \cdot h^{-1}$ purification flow rate, has been verified in test facility ETF-HPS with the purification efficiency greater than 95% [21]. The detailed purification process in the HPS is presented in Figure 1. Helium enters the purification bypass and then proceeds through the dust filter,

Table 1: Material parameters of the monitoring instrument.

	Material parameters	National standards for reference
Insulating layer	Foam glass	GB/T 4132-1996
Γ detector	NaI(Tl) crystal scintillation detector (Φ50 mm × 50 mm), with a 0.5 mm aluminum layer	-
Lead shield cell	Pb: 96%; Sb:4%	GB/T 1470-2014
Tube wall	321 stainless steel	GB/T 20878-2007

copper oxide bed, pipe filter, moisture separator, molecular sieve adsorber, and low-temperature adsorber.

Due to the operation characteristics of pebble-bed reactors, it is difficult to set online monitoring systems to detect the activity concentration of fission products in the core. However, the radioactivity level in the primary loop can reflect the radiation environment in the core. Therefore, the online gross γ monitoring instrument with a high detection range from 3.7×10^7 to 3.7×10^{13} Bq/m^3 was set at the entrance of the HPS, while the online gross γ monitoring with a low detection range from 1×10^5 to 1×10^{11} Bq/m^3 was set at the exit of the HPS. The positions of the two online monitoring systems are also presented in Figure 1. Data from the online gross γ monitoring instrument with a high detection range can indicate the radioactivity level in the primary helium and thus determine the operational status of the fuel elements in the core. Data from the online gross γ monitoring instrument with a low detection range can indicate the radioactivity level in the primary helium after purification. Combining data generated by these two online gross γ monitoring instruments, the purification efficiency of HPS in HTR-PM can be deduced.

These two online monitoring instruments are important components of the process and effluent radiation monitoring systems in HTR-PM which control the gross activity of the primary loop. In this study, we focused on researching the design scheme and detection principle of the online gross γ monitoring instrument with a low detection range at the exit of the HPS. The research on the online gross γ monitoring instrument with a high detection range and its design will be illustrated in another paper.

The online gross γ monitoring instrument is composed of two parts: the detecting section and the in-place disposal box. The detecting section includes an insulating layer, a scintillation detector, and a lead shield cell. The scintillation detector contains a NaI(Tl) crystal, photomultiplier, and preamplifier circuit. The online gross γ monitoring instrument will be installed in the nuclear auxiliary building, with the detector placed directly against the pipe downstream of the low-temperature absorber in the HPS. When the γ rays enter the NaI(Tl) crystal, fluorescence occurs. Subsequently, the light signal is converted into an electrical signal by the photomultiplier. The electrical signal is then sent to the in-place disposal box, where it is amplified. After signal screening and shaping, a standard signal is generated and sent to the scaling circuit for counting. The in-place disposal box displays the activity concentration value on the front panel and determines whether to initiate an alarm signal by comparing the measurement to the preset alarm threshold. In addition, the activity concentration value and the alarm information can be transmitted to the control room using the Modbus communication protocol and/or hardwire.

Relevant material parameters of the monitoring instrument can be seen in Table 1. The configuration of the monitoring instrument is exhibited in Figure 2, and its installation diagram and the in-place disposal box are presented in Figure 3. The online gross γ monitoring instrument has been manufactured in a domestic factory and sent to the worksite for installation. Figure 4 shows the physical map of the online monitoring instrument and its in-place disposal box.

3. Simulation of the Detection Efficiency

We designed this online gross γ monitoring instrument and used the Monte Carlo method to simulate its average detection efficiency. We anticipated that the results of our simulations could offer valuable information when the online gross γ monitor is used during the actual operation of the HTR-PM reactor.

The purification efficiency of HPS in HTR-10 was estimated above 99% [20]. The results of the HTR-PM test facilities project demonstrated a purification efficiency over 95% [21]. In our simulation, we assumed that the activity concentration of the radioactive nuclides in the primary coolant at the exit of the HPS was proportional to the activity concentration in the primary circuit. Considering the average helium purification efficiency, the percentages of the source term nuclides in the primary coolant at the exit of the HPS will be chosen as 0.1, 1, and 5% hereafter. The theoretical calculations of the activity concentration in the primary circuit were adopted from Chapter 11 of the Final Safety Analysis Report for HTR-PM [22].

Table 2 lists the activity concentrations of the radioactive nuclides in the primary coolant which should be considered while using the online gross γ monitoring instrument.

Two parameters K_{Total} and K_{Eff} were used to evaluate detection efficiency. K_{Total} represents the ratio of counts per second in the NaI(Tl) detector to the activity concentration of purified helium over the entire spectrum (energy range from 100 to 3000 keV), which is determined by the characteristics of the reactor, and K_{Eff} is the ratio of count rate to total activity concentration of purified helium in the characteristic spectrum interval of Kr-88 (785–885 keV). Here we chose Kr-88 as the typical nuclide because it seemed to be the most representative nuclide in the primary coolant helium and had the highest activity concentration of all nuclides.

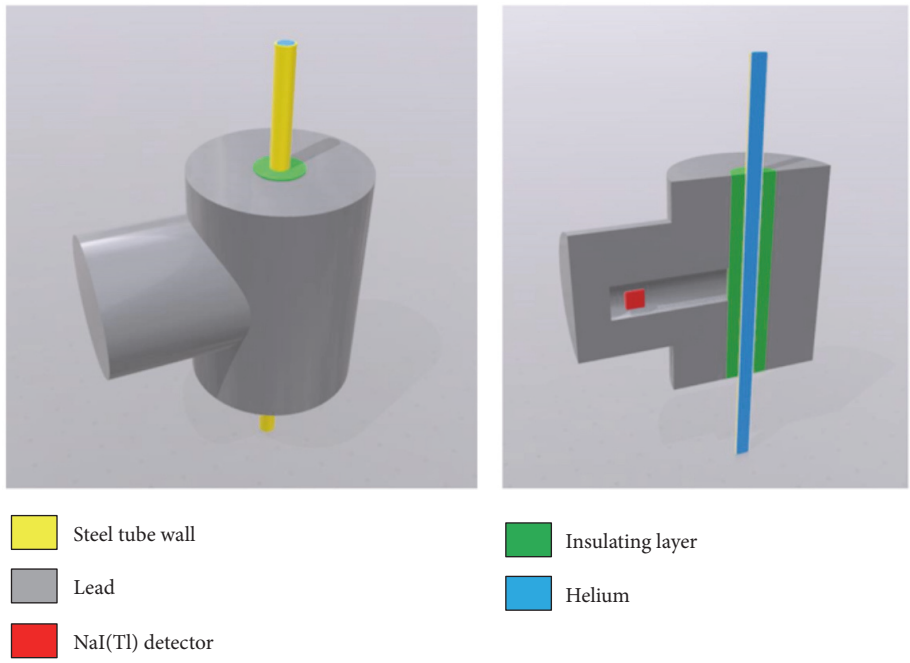

Figure 2: Schematic diagram of the profile and internal structure of the online γ monitoring instrument used at the exit of the HPS.

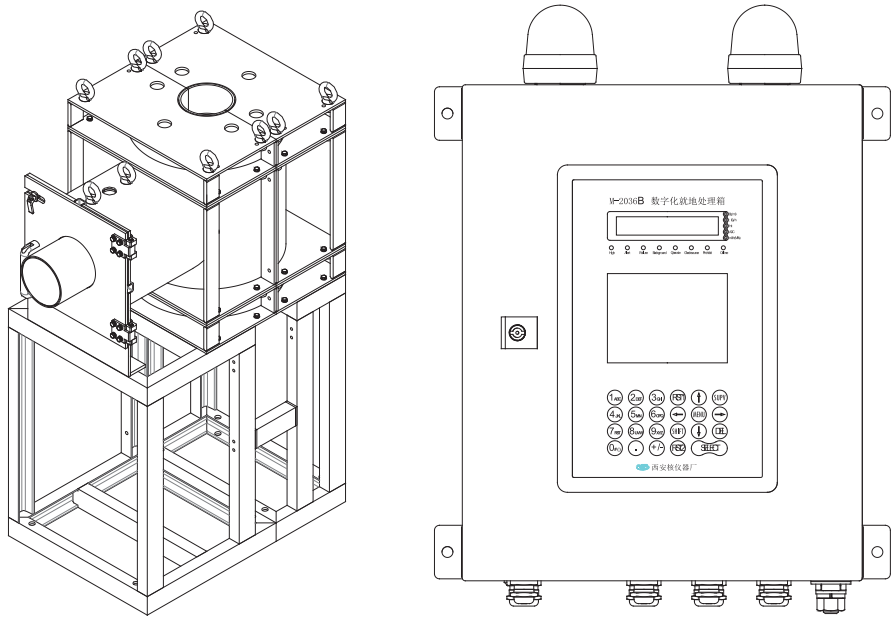

Figure 3: Installation diagram of the online monitoring instrument and in-place disposal box.

Since we chose the NaI(Tl) crystal scintillation detector, which has a large detection range but a relatively poor resolution compared with that of the high-purity germanium (HPGe) detector, the source of the Monte Carlo model was simplified as follows:

(a) To remove the interference and scattering of low energy γ ray, counts lower than 100 keV were omitted

(b) We calculated the product of the activity concentration of each nuclide and its maximum emission probability of γ rays (energy range from 100 to 3000 keV) in one decay. The results are listed in Table 2. For example, the value of the product for Xe-135, 1.17E+02 Bq·L^{-1}, was the largest. If the product of a nuclide was lower than 0.1% of the product of Xe-135, this nuclide would be neglected

(c) Since the half-lives of Kr-90 and Xe-139 were less than 1 min and their products mentioned above were less than 5% of the product of Xe-135, their contributions to photon counting were deemed negligible

Figure 4: Schematic diagrams of the appearance of the online monitoring instrument and its in-place disposal box.

(d) Nuclides released photons with different energies in the decay process and these photons had different branch fractions. By evaluation, we concluded that only the photons that had emission probabilities higher than 1% of the total fractions would contribute to the counting

After the simplification mentioned above, we generated a list of nuclides, including Kr-85m, Kr-87, Kr-88, Kr-89, Xe-133 Xe-133m, Xe-135, Xe-135m, Xe-137, Xe-138, I-131, I-132, I-133, I-134, I-135, Rb-88, and Cs-138, as the source terms for the input of the Monte Carlo model.

Subsequently, we considered Xe-135 as an example to introduce the Monte Carlo simulation. Xe-135 can emit photons with energies of 0.608 and 0.250 MeV, which have probabilities of 0.029 and 0.899, respectively. Therefore, we used these two γ branches as source terms for our calculations. The output data meant the average pulses emitted by the detector owing to the decay of Xe-135 per second. The simulation procedures of other nuclides are almost the same. The detailed results are presented in Table 3.

We used the following equation to calculate the detection efficiency of Xe-135:

$$K_{Xe-135} = C_{Xe-135} \times V_{He} \times I_{Xe-135}. \quad (1)$$

K_{Xe-135} is the detection efficiency of Xe-135 [cps/(Bq · L^{-1})].

C_{Xe-135} is the average pulse emitted by the detector caused by the decay of Xe-135 per incident particle, which is obtained by Monte Carlo simulations [count/particle].

V_{He} is the volume of the primary coolant in the Monte Carlo simulations, and here we adopted $V_{He} = \pi \times 0.2^2 \times 6.16 = 0.7741$L.

I_{Xe-135} means number of emitted photons per decay of Xe-135, which is the sum of all emission probabilities.

The calculation of other nuclides is similar to that of Xe-135. If we want to calculate the detection efficiency in the full spectrum (100 keV–3000 keV), C_i^{Total} which stands for the value of average pulse output from the detector by the nuclide i in the full spectrum (100 keV–3000 keV) will be used. After computing the detection efficiency of each nuclide, we use the following equation to calculate the total detection efficiency, K_{Total}:

$$K_{Total} = \frac{\sum_i \left(K_i^{Total} \times a_i\right)}{a_{All}}, \quad (2)$$

where K_i^{Total} is the detection efficiency of selected nuclides in the full spectrum (100 keV–3000 keV), a_i is the activity concentration of selected nuclides, a_{All} is the total activity concentration of all selected nuclides, and i means the simplification list of nuclides mentioned above.

If we want to calculate the detection efficiency in the characteristic spectrum interval of Kr-88 which is 785 keV–885 keV, C_i^{Eff} which stands for the value of average pulse output from the detector by the nuclide i in the characteristic spectrum interval of Kr-88 (785 keV–885 keV) will be used. Similar to K_{Total}, the effective detection efficiency K_{Total} can be calculated by the following equation:

$$K_{Eff} = \frac{\sum_i \left(K_i^{Eff} \times a_i\right)}{a_{All}}, \quad (3)$$

where K_i^{Eff} is the detection efficiency of selected nuclides in the characteristic spectrum interval of Kr-88 (785 keV–885 keV).

The detailed calculation results are listed in Tables 4 and 5. K_{Total} is calculated as 1.19E-04 cps/(Bq · L^{-1}) under the aforementioned assumption, while K_{Eff} is calculated as 1.88E-06 cps/(Bq · L^{-1}).

4. Discussions

If we assume the purification efficiency as 99.9%, the total detection efficiency that we obtain is 1.19E-04 cps/(Bq/L), and the sum of the activity concentration of selected nuclides is 1462.80 Bq/L. Thus, the detector has about 10 counts per minute. It may be not enough to reflect the real-time changing

Table 2: Specific activity and other relevant information on the fission products at the exit of the HPS (which has 99.9% purification efficiency).

Nuclides	Half life	Specific activity in the coolant at the exit of the HPS a (Bq·L^{-1})	Number of emitted γ rays with energy higher than 100 keV	γ ray energy (higher than 100 keV) where the emission probability is maximum (keV)	Maximum emission probability of γ ray (energy higher than 100keV) η	$a \times \eta$	Status
Kr-83m	1.83 h	1.40E + 01	0			0.00E + 00	Negligible
Kr-85	10.72 a	1.80E − 01	1	513.99	0.0043	7.81E − 04	Negligible
Kr-85m	4.48 h	6.00E + 01	4	151.18	0.7528	4.52E + 01	
Kr-87	76.3 min	6.70E + 01	22	402.58	0.4950	3.32E + 01	
Kr-88	2.84 h	1.40E + 02	50	2392.10	0.3460	4.84E + 01	
Kr-89	3.16 min	2.00E + 01	141	220.90	0.2000	4.00E + 00	
Kr-90	32.32 s	5.00E + 00	64	1118.70	0.3730	1.87E + 00	Negligible
Xe-131m	11.84 d	4.10E + 00	1	163.93	0.0196	8.04E − 02	Negligible
Xe-133	5.245 d	8.50E + 02	1	177.70	0.0007	6.05E − 01	
Xe-133m	2.19 d	2.80E + 01	1	233.22	0.1030	2.88E + 00	
Xe-135	9.11 h	1.30E + 02	6	249.79	0.8990	1.17E + 02	
Xe-135m	15.36 min	1.40E + 01	1	526.56	0.8100	1.13E + 01	
Xe-137	3.83 min	4.20E + 01	12	455.49	0.3070	1.29E + 01	
Xe-138	14.13 min	9.30E + 01	43	258.31	0.3150	2.93E + 01	
Xe-139	39.68 s	9.10E + 00	≥3	218.59	0.5600	5.10E + 00	Negligible
I-131	8.04 d	1.80E − 01	9	364.48	0.8116	1.46E − 01	
I-132	2.3 h	2.30E + 00	65	667.69	0.9870	2.27E + 00	
I-133	20.8 h	9.20E − 01	22	529.87	0.8632	7.94E − 01	
I-134	52.6 min	4.70E + 00	69	847.02	0.9541	4.48E + 00	
I-135	6.61 h	1.40E + 00	46	1260.40	0.2861	4.01E − 01	
Sr-89	50.55 d	6.60E − 05	1	909.10	0.0002	9.90E − 09	Negligible
Sr-90	28.6 d	4.30E − 07	0			0.00E + 00	Negligible
Cs-134	2.062 a	3.80E − 04	10	604.70	0.9760	3.71E − 04	Negligible
Cs-137	30.17 a	4.90E − 04	≥2	661.66	0.8495	4.16E − 04	Negligible
Ag-110m	249.85 d	3.20E − 04	22	657.75	0.9439	3.02E − 04	Negligible
Co-60	5.271 a	1.10E − 04	3	1173.20 1332.50	1.0000	1.10E − 04	Negligible
Fe-55	2.7 a	4.90E − 06	0			0.00E + 00	Negligible
Cr-51	27.704 d	1.60E − 06	1	320.08	0.0983	1.57E − 07	Negligible
Na-24	15 h	1.00E − 06	3	1368.50	1.0000	1.00E − 06	Negligible
Si -31	157.3 min	4.50E − 09	1	1266.10	0.0007	3.15E − 12	Negligible
K-42	12.36 h	8.20 − 08	3	1524.70	0.1790	1.47E − 08	Negligible
V-52	3.75 min	4.30E − 10	4	1434.10	1.0000	4.30E − 10	Negligible
Mn-54	312.7 d	7.00E − 08	1	834.83	0.9998	7.00E − 08	Negligible
Mn-56	2.5785 h	1.30E − 07	8	846.75	0.9887	1.29E − 07	Negligible
Fe-59	44.63 d	8.30E − 08	6	1099.20	0.5650	4.69E − 08	Negligible
Co-58	70.8 d	8.20E − 08	4	810.76	0.9943	8.15E − 08	Negligible
Co-60m	10.47 min	1.00E − 08	2	1332.50	0.0024	2.40E − 11	Negligible
Ni-63	100.1 a	1.10E − 07	0			0.00E + 00	Negligible
Cu-64	12.701 h	5.10E − 07	2	511.00	0.3574	1.82E − 07	Negligible
Cu-66	5.12 min	7.90E − 10	≥3	1039.20	0.0923	7.29E − 11	Negligible
Mo-99	66.02 h	1.20E − 07	7	739.58	0.1280	1.54E − 08	Negligible
Tc-99m	6.02 h	1.00E − 08	2	140.51	0.8907	8.91E − 09	Negligible
Rb-88	17.8 min	7.70E + 00	15	1836.00	0.2140	1.65E + 00	
Cs-138	32.2 min	1.60E + 00	48	1435.90	0.7630	1.22E + 00	
C-14	5073 a	5.20E − 01	0			0.00E + 00	Negligible
H-3	12.28 a	2.10E + 02	0			0.00E + 00	Negligible

Table 3: Monte Carlo simulation results of selected nuclides.

Nuclides	Average pulses emitted by the detector over the entire spectrum (100–3000 keV) C_i^{Total} (count/particle)	Average pulses emitted by the detector in the characteristic spectrum interval of Kr-88 (785–885 keV) C_i^{Eff} (count/particle)	Estimated relative error	Estimated variance of the variance
Kr-85m	2.674E – 04	0.00E + 00	0.0273	0.0007
Kr-87	4.102E – 04	7.00E – 06	0.0221	0.0005
Kr-88	4.302E – 04	1.28E – 05	0.0216	0.0005
Kr-89	4.050E – 04	7.20E – 06	0.0222	0.0005
Xe-133	2.738E – 04	0.00E + 00	0.0270	0.0007
Xe-133m	3.194E – 04	0.00E + 00	0.0250	0.0006
Xe-135	3.312E – 04	0.00E + 00	0.0246	0.0006
Xe-135m	3.760E – 04	0.00E + 00	0.0231	0.0005
Xe-137	3.700E – 04	2.00E – 07	0.0232	0.0005
Xe-138	3.948E – 04	2.60E – 06	0.0225	0.0005
I-131	3.536E – 04	0.00E + 00	0.0238	0.0006
I-132	4.040E – 04	3.00E – 06	0.0222	0.0005
I-133	3.804E – 04	5.80E – 06	0.0229	0.0005
I-134	4.084E – 04	3.16E – 05	0.0221	0.0005
I-135	4.344E – 04	1.52E – 05	0.0215	0.0005
Rb-88	4.488E – 04	7.00E – 06	0.0211	0.0004
Cs-138	3.616E – 04	0.00E + 00	0.0235	0.0006

Table 4: Calculation of the detection efficiency of the online monitoring system over the entire spectrum (100–3000 keV).

Nuclides	Average pulses emitted by the detector C_i^{Total} (count/particle)	Total γ branch ratio I(number of emitted photons per decay)	Detection efficiency K_i^{Total}[cps/(Bq · L^{-1})]	Activity concentration in the coolant in the exit of helium purification system (99.9% purification efficiency) a_i (Bq·L^{-1})	$K_i^{Total} \times a_i$
Kr-85m	2.674E – 04	0.892670	1.848E – 04	60.00	1.11E – 02
Kr-87	4.102E – 04	0.779675	2.476E – 04	67.00	1.66E – 02
Kr-88	4.302E – 04	1.239245	4.127E – 04	140.00	5.78E – 02
Kr-89	4.050E – 04	1.272980	3.991E – 04	20.00	7.98E – 03
Xe-133	2.738E – 04	0.000712	1.509E – 07	850.00	1.28E – 04
Xe-133m	3.194E – 04	0.103000	2.547E – 05	28.00	7.13E – 04
Xe-135	3.312E – 04	0.927948	2.379E – 04	130.00	3.09E – 02
Xe-135m	3.760E – 04	0.809970	2.358E – 04	14.00	3.30E – 03
Xe-137	3.700E – 04	0.320150	9.170E – 05	42.00	3.85E – 03
Xe-138	3.948E – 04	1.133639	3.465E – 04	93.00	3.22E – 02
I-131	3.536E – 04	0.962891	2.636E – 04	0.18	4.74E – 05
I-132	4.040E – 04	2.870846	8.978E – 04	2.30	2.06E – 03
I-133	3.804E – 04	0.991557	2.920E – 04	0.92	2.69E – 04
I-134	4.084E – 04	2.885958	9.124E – 04	4.70	4.29E – 03
I-135	4.344E – 04	1.214136	4.083E – 04	1.40	5.72E – 04
Rb-88	4.488E – 04	0.373961	1.299E – 04	7.70	1.00E – 03
Cs-138	3.616E – 04	1.872362	5.241E – 04	1.60	8.39E – 04
K_{Total}			1.19E – 04		

Table 5: Calculation of the detection efficiency of the online monitoring system in the characteristic spectrum interval of Kr-88 (785–885 keV).

Nuclides	Average pulses emitted by the detector in the characteristic spectrum interval of Kr-88 (785–885 keV) C_i^{Eff} (count/particle)	Total γ branch ratio $\boldsymbol{I}$ (number of emitted photons per decay)	Detection efficiency K_i^{Eff} [cps/(Bq · L^{-1})]	Specific activity in the coolant at the exit of the HPS (99.9% purification efficiency) a_i(Bq·L^{-1})	$K_i^{Eff} \times a_i$
Kr-85m	0.00E + 00	0.892670	0.00E + 00	60.00	0.00E + 00
Kr-87	7.00E – 06	0.779675	4.22E – 06	67.00	2.83E – 04
Kr-88	1.28E – 05	1.239245	1.23E – 05	140.00	1.72E – 03
Kr-89	7.20E – 06	1.272980	7.09E – 06	20.00	1.42E – 04
Xe-133	0.00E + 00	0.000712	0.00E + 00	850.00	0.00E + 00
Xe-133m	0.00E + 00	0.103000	0.00E + 00	28.00	0.00E + 00
Xe-135	0.00E + 00	0.927948	0.00E + 00	130.00	0.00E + 00
Xe-135m	0.00E + 00	0.809970	0.00E + 00	14.00	0.00E + 00
Xe-137	2.00E – 07	0.320150	4.96E – 08	42.00	2.08E – 06
Xe-138	2.60E – 06	1.133639	2.28E – 06	93.00	2.12E – 04
I-131	0.00E + 00	0.962891	0.00E + 00	0.18	0.00E + 00
I-132	3.00E – 06	2.870846	6.67E – 06	2.30	1.53E – 05
I-133	5.80E – 06	0.991557	4.45E – 06	0.92	4.10E – 06
I-134	3.16E – 05	2.885958	7.06E – 05	4.70	3.32E – 04
I-135	1.52E – 05	1.214136	1.43E – 05	1.40	2.00E – 05
Rb-88	7.00E – 06	0.373961	2.03E – 06	7.70	1.56E – 05
Cs-138	0.00E + 00	1.872362	0.00E + 00	1.60	0.00E + 00
K_{Eff}			1.88E – 06		

condition of the activity concentration in the primary loop. However, when the purification efficiency of HPS gets worse and is degenerated to 95%, we will have 500 counts per minute. The counting rate will increase 50 times compared to the previous situation. Since this online gross γ monitoring instrument is set at the exit of HPS, the main function for this instrument is to monitor the purification efficiency of the HPS. If the purification efficiency of the HPS of HTR-PM degenerated from 99.9% to 95%, the counting rate of this instrument will increase 50 times based on current simulations. Therefore, the monitoring function can be realized to ensure the normal operation of the HPS.

Since current Monte Carlo simulation results are based on the source term calculations in the primary loop of HTR-PM, the actual source term during the operation of HTR-PM may vary from the current hypothesis. Thus, we change the proportion of source term nuclides to analyze variation of the detection efficiency in full spectrum and in the Kr-88 characteristic spectrum interval. According to (2), the total detection is affected by both activity concentration and a single nuclide's detection efficiency. The detection efficiency of each nuclide in full spectrum (100 keV–3000 keV) is almost at the same order of magnitude, while the activity concentration of each is quite different. In the characteristic spectrum interval of Kr-88 (785 keV–885 keV), nuclides' detection efficiencies are in a different order of magnitude.

Kr-88, Xe-133, and Xe-135 are the nuclides with the three greatest activity concentrations, and I-131 has the lowest activity concentration. In a given 99.9% purification efficiency, the activity concentrations of all selected nuclides can be seen in Table 4. To increase or decrease some nuclides' activity concentrations such as the three nuclides mentioned above by one order of magnitude, the variation of K_{Total} and K_{Eff} due to the change on the relative proportion of nuclides' activity concentrations has been calculated, which is listed in Table 6.

The result indicates that changes on the nuclides with higher activity concentrations lead to more evident changes on K_{Total} and K_{Eff}, while the nuclides with low activity concentration like I-131 have little influence on K_{Total} and K_{Eff}. Since $K_{\mathrm{Kr-88}}^{Total} > K_{Total}$, as a result, the increase of Kr-88 fraction leads to the increase of K_{Total}. While $K_{\mathrm{Xe-133}}^{Total} << K_{Total}$, the increase of Xe-133 proportion leads to the decrease of K_{Total}. The results also indicate that K_{Eff} is more sensitive to the change of related nuclide concentrations compared with K_{Total}.

The counting rate should be controlled in an acceptable range so that we can increase the precision of the result. The maximum counting rate of this monitoring instrument should be 10^5 per second, which is much higher than our existing counting rate, while the minimum counting rate depends on the effect of the environment radiation. The environment background radiation in the helium purification

Table 6: Changes in K_{Total} and K_{Eff} due to increasing or decreasing the activity concentrations of some nuclides by one order of magnitude.

		K_{Total} [cps/(Bq · L^{-1})]	Relative rate of change (%)	K_{Eff} [cps/(Bq · L^{-1})]	Relative rate of change (%)
Original activity concentration		1.19E − 04	0.0	1.88E − 06	0.0
Kr-88	Increase its activity concentration by one order of magnitude	2.55E − 04	114.3	6.69E − 06	255.9
	Decrease its activity concentration by one order of magnitude	9.10E − 05	−23.5	8.96E − 07	−52.3
Xe-133	Increase its activity concentration by one order of magnitude	1.92E − 05	−83.9	3.01E − 07	−84.0
	Decrease its activity concentration by one order of magnitude	2.49E − 04	109.2	3.93E − 06	109.0
Xe-135	Increase its activity concentration by one order of magnitude	1.72E − 04	44.5	1.04E − 06	−44.7
	Decrease its activity concentration by one order of magnitude	1.08E − 04	−9.2	2.04E − 06	8.5
I-131	Increase its activity concentration by one order of magnitude	1.19E − 04	0.0	1.87E − 06	−0.5
	Decrease its activity concentration by one order of magnitude	1.19E − 04	0.0	1.88E − 06	0.0

Table 7: Detection efficiency of Kr-88 and Xe-135 for different NaI(Tl) crystal sizes and distances between crystal and pipe.

Size of the NaI crystal		Φ80 mm × 50 mm	Φ60 mm × 50 mm	Φ50 mm × 50 mm	Φ50 mm × 50 mm	Φ50 mm × 50 mm
Distance between the NaI crystal center and pipe center [cm]		35.15	35.15	35.15	30.15	20.15
Kr-88	C^{Total}_{Kr-88} [count/particle]	1.02E – 03	6.00E – 04	4.30E – 04	6.33E – 04	1.82E – 03
	C^{Eff}_{Kr-88} [count/particle]	3.46E – 05	1.92E – 05	1.28E – 05	1.80E – 05	4.16E – 05
Xe-135	C^{Total}_{Xe-135} [count/particle]	7.99E – 04	3.31E – 04	4.64E – 04	4.89E – 04	1.38E – 03
	C^{Eff}_{Xe-135} [count/particle]	0	0	0	0	0

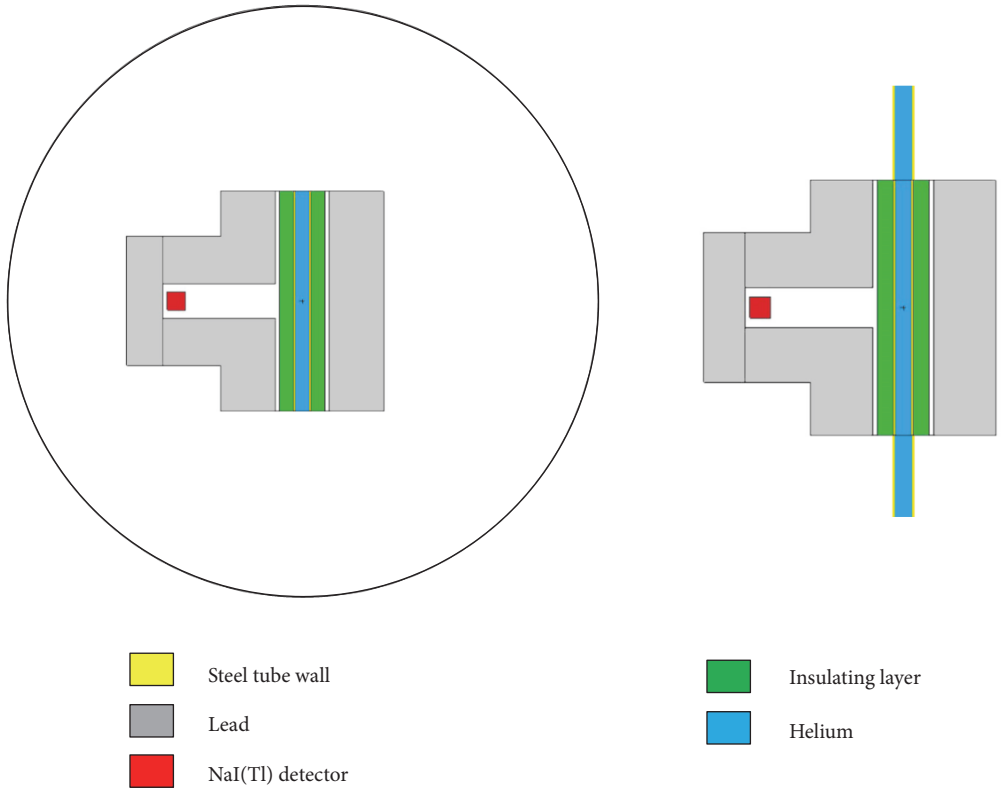

Figure 5: Monte Carlo simulation model and real-life situation of the online monitoring instrument.

system room in HTR-PM is less than 3 mGy/h at the position of the monitoring instrument. Since we have set a lead shield cell around the monitoring instrument, the background noise is neglected here.

The simulation results mentioned above show that there are only 10 counts per second under the assumption of 99.9% purification efficiency. Since the counting rate is small, we can improve the counting rate by increasing the volume of NaI(Tl) crystal or shorten the distance between detector and pipe. Table 7 shows that detection efficiency is significantly improved by these two methods. By increasing the diameter of NaI(Tl) crystal from 50 mm to 80 mm, C^{Total}_{Kr-88}, C^{Eff}_{Kr-88}, and C^{Total}_{Xe-135} have nearly doubled. By shortening the distance between the NaI(Tl) crystal and measured pipe center from 35.15 mm to 20.15 mm, C^{Total}_{Kr-88}, C^{Eff}_{Kr-88}, and C^{Total}_{Xe-135} have almost tripled. C^{Eff}_{Xe-135} is always zero and does not change with the different sizes and distances, which means that Xe-135 has no contribution to the count in the characteristic spectrum interval of Kr-88 (785 keV–885 keV).

Note that the distance between the NaI(Tl) crystal and measured pipe center cannot be reduced infinitely. As Figure 5 shows, the Monte Carlo simulation model neglects the influence of the nonmeasured pipe section and assumes its radiation is fully shielded by lead. If the distance continues to be reduced, the lead shield will be less effective and the results will be biased.

The scintillation detector contains a NaI(Tl) crystal, a photomultiplier, and a preamplifier circuit. The output of the existing instrument is the total pulse counts. But a continuous spectrum can be obtained if nuclide identification function is required. The high-purity germanium (HPGe) detector has a smaller full width at half maximum (FWHM) compared with that of the NaI(Tl) detector, which means a better revolution.

In the future, the HPGe detector may be a choice to realize the online monitoring of the source term in the primary loop with the nuclide identification function.

5. Conclusion

The online gross γ monitoring instrument which can be used to reflect the radioactivity level in the primary helium and evaluate the purification of HPS has been designed and installed at the exit of HPS in HTR-PM. A Monte Carlo method has been adopted to simulate the detection efficiency of the monitoring instrument. The simulation result shows that the detection efficiency of the monitoring instrument is around 10 pulses per minute under the 99.9% purification efficiency assumption. If the purification efficiency deteriorates to 95%, the counting rate will increase 50 times, which means that it is feasible to detect the deterioration of the helium purification system.

Based on the sensitivity analysis, the detection efficiency is sensitive to the fraction of nuclides. The nuclides with relatively higher activity concentration have a greater effect on K_{Total} and K_{Eff}. K_{Eff} is more sensitive to the change of a typical nuclide's concentration, such as Kr-88, I-134, and I-135, while K_{Total} exhibited less effect from the concentration variation of the nuclides in the primary loop. Enlarging the detector volume or shortening the distance between the detector and the pipe can improve the detection efficiency evidently.

When the HTR-PM starts to operate, this monitoring instrument can be calibrated accurately and shows a digital signal which can reflect timely condition. The current research can supply useful understanding of the radiation monitoring of source terms in the primary loop of HTR-PM and provide important reference for the application of online monitoring instrument in HTGRs.

Data Availability

The data in text format used in support of the findings of this study are available from the corresponding author upon request.

Conflicts of Interest

The authors declare that they have no conflicts of interest.

Acknowledgments

This work was supported by the National Natural Science Foundation of China (No. 11575099), the National S&T Major Project (Grant No. ZX069), the Major National R&D Projects (2013ZX06002001-014), and the Tsinghua University Initiative Scientific Research Program (No. 20151080375). We are grateful for the fruitful discussions with Prof. Weimin Ma in the Division of Nuclear Power Safety, Royal Institute of Technology (KTH), Stockholm, Sweden.

References

[1] U. S. DOE Nuclear Energy Research Advisory Committee (NERAC) and the Generation IV International Forum (GIF), A technology roadmap for generation IV nuclear energy systems, GIF-002-00.

[2] M. Schneider, A. Froggatt et al., "The World Nuclear Industry Status Report 2017," 2017.

[3] Z. Zhang, Z. Wu, D. Wang et al., "Current status and technical description of Chinese 2 × 250 MWth HTR-PM demonstration plant," *Nuclear Engineering and Design*, vol. 239, no. 7, pp. 1212–1219, 2009.

[4] Z. Zhang, H. Wang, Y. Dong, and F. Li, "Future Development of Modular HTGR in China after HTR-PM," in *Proceedings of the HTR 2014*, Paper HTR2014-11456, 2014.

[5] Z. Wu, D. Lin, and D. Zhong, "The design features of the HTR-10," *Nuclear Engineering and Design*, vol. 218, pp. 25–32, 2002.

[6] Z. Xiangwen, L. Zhenming, Z. Jie et al., "Preparation of spherical fuel elements for HTR-PM in INET," *Nuclear Engineering and Design*, vol. 263, pp. 456–461, 2013.

[7] H. M. Hashemian, "On-line monitoring applications in nuclear power plants," *Progress in Nuclear Energy*, vol. 53, no. 2, pp. 167–181, 2011.

[8] S. J. Livingstone, *Development of an on-line fuel failure monitoring system for CANDU reactor [Ph.D. thesis]*, Royal Military College of Canada, Kingston, Canada, 2012.

[9] J. K. Hartwell, D. M. Scates, and M. W. Drigert, "Design of an on-line, multi-spectrometer Fission Product Monitoring System (FPMS) to support Advanced Gas Reactor (AGR) fuel testing and qualification in the advanced test reactor," in *Proceedings of the Nuclear Science Symposium Conference Record, 2005 IEEE*, pp. 1168–1172, Puerto Rico, October 2005.

[10] F. Xie, W. Li, Z. Li et al., "Design of the Process and Effluent Radiation Monitoring System of HTR-PM," in *Proceedings of the 2016 24th International Conference on Nuclear Engineering*, Charlotte, North Carolina, USA, 2016.

[11] F. Xie, J. Cao, X. Feng et al., "Study of tritium in the primary loop of HTR-10: experiment and theoretical calculations," *Progress in Nuclear Energy*, vol. 105, pp. 99–105, 2018.

[12] F. Xie, J.-Z. Cao, Z.-P. Chen, and Y.-J. Dong, "Design and study of radioactive graphite dust experimental system in primary loop of HTR-10," *Atomic Energy Science and Technology*, vol. 49, no. 4, pp. 744–749, 2015 (Chinese).

[13] F. Xie, J. Cao, X. Feng et al., "Experimental research on the radioactive dust in the primary loop of HTR-10," *Nuclear Engineering and Design*, vol. 324, pp. 372–378, 2017.

[14] W. Peng, Q. Sun, F. Xie, and Y. Jiang, "Simulations of the dust behavior in the sampling and dust filters in the primary loop of HTR-10," *Nuclear Engineering and Design*, vol. 340, pp. 112–121, 2018.

[15] F. Xie, H. Li, X. Liu et al., "A comprehensive study on source terms in irradiated graphite spheres of HTR-10," *Annals of Nuclear Energy*, vol. 122, pp. 352–365, 2018.

[16] H. Li, X. Liu, F. Xie, and F. Jia, "Experimental study on the content and distribution of key nuclides in an irradiated graphite sphere of HTR-10," *Nuclear Engineering and Design*, vol. 323, pp. 39–45, 2017.

[17] S. Wang, Y. Pi, F. Xie, H. Li, and J. Cao, "Study on ^{14}C content in post-irradiation graphite spheres of HTR-10," *Atomic Energy Science and Technology*, vol. 48, pp. 506–510, 2014 (Chinese).

[18] M. Lou, W. Li, F. Xie et al., "Design of the sampling measurement and radiochemistry lab in the nuclear island of HTR-PM," in *Proceedings of the 2018 26th International Conference on Nuclear Engineering*, London, England, 2018.

[19] J. Cao, L. Zhang, F. Xie, B. Xia, and S. Lam, "Source term study on tritium in HTR-PM: theoretical calculations and experimental design," *Science and Technology of Nuclear Installations*, vol. 2017, Article ID 3586723, 11 pages, 2017.

[20] M. S. Yao, R. P. Wang, Z. Y. Liu, X. D. He, and J. Li, "The helium purification system of the HTR-10," *Nuclear Engineering and Design*, vol. 218, no. 1-3, pp. 163–167, 2002.

[21] Z. Zhang, Y. Dong, F. Li et al., "The Shandong Shidao Bay 200 MWe high-temperature gas-cooled reactor pebble-bed module (HTR-PM) demonstration power plant: an engineering and technological innovation," *Engineering*, vol. 2, no. 1, pp. 112–118, 2016.

[22] Z. Zhang, Y. Dong, and J. Huang, *Final Safety Analysis Report of the High Temperature Gas-Cooled Reactor Pebble-Bed Module (HTR-PM)*, Institute of Nuclear and New Energy Technology, Tsinghua University, Beijing, China, 2016.